Skyrmion-induced localized state in a two-dimensional superconductor

Sergey S. Pershoguba[1], Sho Nakosai[1,2], and Alexander V. Balatsky[1,3]
[1] *Nordita, Center for Quantum Materials, KTH Royal Institute of Technology, and Stockholm University, Roslagstullsbacken 23, S-106 91 Stockholm, Sweden*
[2] *Condensed Matter Theory Laboratory, RIKEN, Wako, Saitama, 351–0198, Japan and*
[3] *Institute for Materials Science, Los Alamos National Laboratory, Los Alamos, NM 87545, USA*
(Dated: October 16, 2015)

We consider a superconductor proximity coupled to a 2D ferromagnetic film with a topological configuration of the ferromagnetic vector, i.e., the skyrmion. Using the T-matrix calculations as well as well numerical modeling we calculate the spin-polarized local density of states (SP-LDOS) in the vicinity of the skyrmion. We identify a skyrmion-induced Yu-Shiba-Rusinov (s-YSR) bound state, calculate its energy and a spectral width. We predict that sYSR resonance has a spatial power-law decay. This implies that superconductivity could facilitate a long-range interaction between distinct skyrmions on the surface of the ferromagnetic film.

Introduction. General context of skyrmions asd tolopolical excitations: memory, manipulation, local creation via SP STM. Extension of skyrmion discussion to the case of hybrid structures: SC and Skyrmion. What are the consequenc of brining topological exchange field into SC. Question we address is the possible local spectroscopic signatures of SC quasiparticles in SC due to skyrmion field. We know from the past discussion that there are impurity bound states in SC near magnetic impurities. We have now the framework to address formation of bound states. Talk about local single impurity limit (YSR) and show the cartoon of the local and extended skyrmion and spectra. Main section: There are two effects: local scattering and Zeeman field hence the DOS will be split etc. Draw similarities and differences with single imp. In parallel with skyrmion discovery the local imaging using magnetic probes like MFM and SP-STM allowed one to image the matter at atomic resolution while also resolving spin content of electron carriers in the substrate. Here we prove the existence of the new type of localized excitation on the skyrmion core we call Sc-YSR state (alternative is skyrmion bound state (sbs)). Show the main results upfront in the introduction. Both LDOS and SP-LDOS.

It has been pointed out over the past few years [1, 2] that superconductivity can facilitate strong long-range interaction between the magnetic impurities. Maybe the same thin will happen for skyrmions.

Skyrmions in Wiesendanger's group [3–9]. .

Introduce T matrix and results for analytic solution. Introduce the numerical approach and presenst the results oas a function of position and as a function of energy. Kind of same figs as in Shos talk. Discuss the results and what it means, how big the signal is etc. Unfortunately we do not see any topological state at zero energy and as such these result represent a new kind of magnetic texture induced states that exhibit intragap states.

Skyrmions in ferromagnetic films. Let the three-dimensional vector $S(\boldsymbol{r}) = (S_x, S_y, S_z)$ describe the configuration of the ferromagnetic vector in a two-dimensional ferromagnetic film $\boldsymbol{r} = (x, y)$. The configurations of the field $S(\boldsymbol{r})$ shown in Fig. 1(a) and (b) are referred to as skyrmions. The skyrmion configuration of the field is characterized by the topological charge

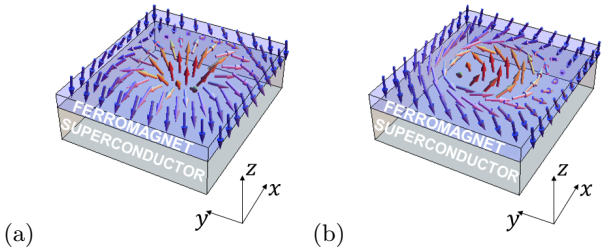

FIG. 1. (Color online.) Ferromagnetic film deposited on top of a superconductor. The ferromagnetic vector has skyrmion configuration. (a) Hedgehog skyrmion. (b) Spiral skyrmion.

$$Q = \frac{1}{4\pi}\int d^2r\, \hat{\boldsymbol{S}}\cdot(\nabla_x\hat{\boldsymbol{S}}\times\nabla_y\hat{\boldsymbol{S}}), \quad \hat{\boldsymbol{S}} = \frac{\boldsymbol{S}}{S}, \tag{1}$$

which cannot be altered by the continuous transfomation of the field. We also characterize the skyrmion fields by the zeroth and first moments

$$S_i^{(0)} = \int d^2r\, \left[S_i(\boldsymbol{r}) - S_i(\infty)\right],\ i \in \{x, y, z\}, \tag{2}$$

$$S_{ij}^{(1)} = \int d^2r\, \left[S_i(\boldsymbol{r}) - S_i(\infty)\right] r_j,\ j \in \{x, y\}. \tag{3}$$

The zeroth moment $\boldsymbol{S}^{(0)} = S_{\rm e}\hat{\boldsymbol{z}}$ characterizes the effective out-of-plane magnetic moment of the skyrmion and is equal for the two skyrmions shown in Fig. 1(a) and (b). Whereas, the first-order moment $S_{ij}^{(1)}$ characterizes the in-plane pattern of the ferromagnetic vector $\boldsymbol{S}(\boldsymbol{r})$. Note that for the cylindrically symmetric field $S(\boldsymbol{r})$, the first order moment defined in Eq. (3) can be expanded in the symmetric and antisymmetric parts

$$S_{ij}^{(1)} = S_{\rm m}\,\delta_{ij} + S_{\rm a}\,\epsilon_{ijz} \tag{4}$$

The skyrmions shown in Fig. 1(a) and (b) have monopole $S_{\rm m}$ and anapole $S_{\rm a}$ moments correspondingly, hence the

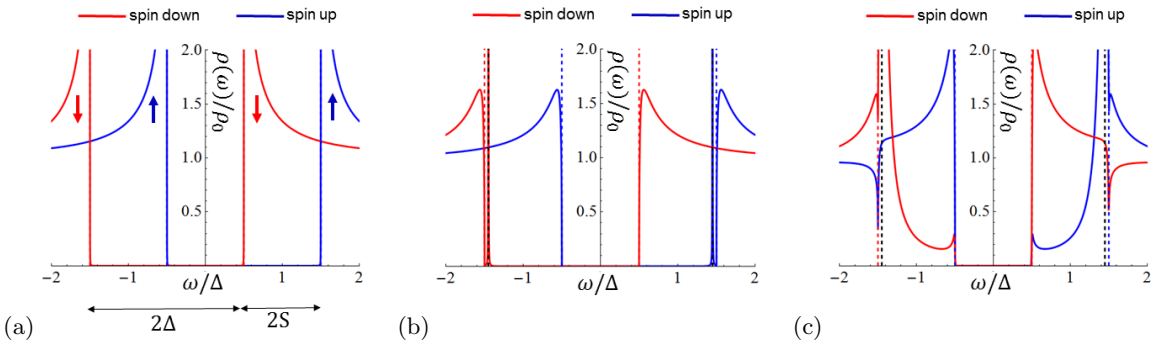

FIG. 2. (Color online) Spin-polarized local density of states (a) away from the skyrmion and (b,c) at the core of the skyrmion. Panel (b) corresponds to the usual T-matrix that takes into account only out-of-plane. Panel (c) corresponds to the T-matrix that takes into account in-plane spin. Comparing (b) and (c) notice that a thin YSR state in (b) becomes a thick resonance in (c). The parameters of plots are $2S = \Delta = 0.25E_F$ and $R = 1/p_F = \xi/8$. Blue and red dashed lines indicate the positions of the shifted spin-up and spin-down bands, respectively. The black dashed line indicates the position of the YSR pole, given by Eq. .

name of the skyrmions. However the two types of the skyrmions have the same topological charge (1) and can be continuosly deformed into each other.

Model The model is given by the following 4-by-4 Bogolyubov-de Gennes (BdG) Hamiltonian

$$H = \xi(\boldsymbol{p})\tau_z + \Delta\tau_x - \boldsymbol{S}(\boldsymbol{r})\cdot\boldsymbol{\sigma}, \tag{5}$$

$$\xi(\boldsymbol{p}) = \frac{p^2}{2m} - \mu, \quad \boldsymbol{p} = -i(\nabla_x, \nabla_y), \tag{6}$$

which describes the proximity coupling of the ferromagnetic vector $S(\boldsymbol{r})$ to the itinerant electrons of a two-dimensional (2D) superconductor with the superconducting gap Δ. The Pauli matrices $\boldsymbol{\tau}$ and $\boldsymbol{\sigma}$ act, respectively, in the particle-hole and spin subspaces of the four-component spinor $\Psi = (\psi_\uparrow, \psi_\downarrow, \psi_\downarrow^\dagger, -\psi_\uparrow^\dagger)^T$. For simplicity, we assume that the magnitude of the superconductor-ferromagnet coupling is constant and only the direction $\boldsymbol{S}(\boldsymbol{r})$ varies, i.e., we set $\boldsymbol{S}(\boldsymbol{r}) = S\,\boldsymbol{n}(\boldsymbol{r})$, where $\boldsymbol{n}$ is a unit vector. In order to proceed further let compare the typical lengthscales. The radius of skyrmions R found in experiments [3–9] does not typically exceed 5 nm, whereas the superconducting coherence length ξ_{sc} varies largely from a micron to a few nanometers as in, e.g., curprates. For the analysis below, we assume the superconducting coherence length much larger $\xi_{sc} \gg R$, and briefly comment about the opposite limit in the Supplemental Material (Shall we discuss this? Local gauge transform and introduce effective spin-orbit, etc.). In the chosen limit the superconductivity cannot "resolve" the fine details of the field $\boldsymbol{S}(\boldsymbol{r})$ and only "sees" as a skyrmion as local magnetic defect. Therefore we shall apply a Yu-Shiba-Rusinov [10–13] treatment the skyrmion as a local impurity.

T-matrix analysis Superconductor-ferromagnet heterostructures were recently proposed as a viable platform for realizing topological superconductivity (TS) [**? ? ?**], which can host Majorana fermion quasiparticles at vortex cores and boundaries [**? ? ?**]. Majorana fermions obey non-Abelian statistics and may be utilized for topological quantum computation [**? ? ?**]. The key ingredients driving these systems in the topologically non-trivial regime are the spin-orbit coupling (SOC) and magnetism. Recently, the search for experimental realizations of TS has also led to engineering the impurity bands of the Yu-Shiba-Rusinov (YSR) states [10–12], induced by magnetic atoms on the surface of a superconductor [14**? ? ? ? ? ? ? ? ? ? ? ?**]. Following this recipe, zero-energy peaks in the tunneling spectrum were recently measured at the ends of a one-dimensional (1D) chain of magnetic atoms [**?**]. Such a tunneling spectrum could be the evidence of Majorana edge states, although alternative explanations are also possible [**?**].

It is convenient to split the Hamiltonian (5) $H = h(\boldsymbol{p}) + V(\boldsymbol{r})$ into the spatially uniform part $h(\boldsymbol{p})$ and a local perturbation $V(\boldsymbol{r})$ describing the skyrmion

$$h(\boldsymbol{p}) = \xi(\boldsymbol{p})\tau_z + \Delta\tau_x - \boldsymbol{S}(\infty)\cdot\boldsymbol{\sigma}, \quad \boldsymbol{S}(\infty) = -S\,\hat{\boldsymbol{z}} \tag{7}$$

$$V(\boldsymbol{r}) = -\left[\boldsymbol{S}(\boldsymbol{r}) - \boldsymbol{S}(\infty)\right]\cdot\boldsymbol{\sigma} \tag{8}$$

For the skyrmions shown in Figs. 1(a) and (b), the ferromagnetic vector is $S(\infty) = -S\,\hat{\boldsymbol{z}}$ far from skyrmion, and is parallel to $\boldsymbol{S}(0) = S\hat{\boldsymbol{z}}$ at the skyrmion core. The Hamiltonian $h(\boldsymbol{p})$ describes a superconductor proximity coupled to a ferromagnet with constant magnetization, i.e. in the absence of the skyrmion. The ferromagnetic term $S\sigma_z$ breaks two-fold Kramers degeneracy of the bands and the spectrum contains four coherence peaks with energies $\pm\Delta \pm S$ as shown in Fig. (2)(a). The bands corresponding to opposite spin are decoupled. The spectrum maintains a gap as long as the Zeeman coupling is less than the superconducting gap, i.e. $S < \Delta$. Such spectrum should be possible to detect by the spin-polarized tunneling spectroscopy methods[cite relevant papers]. In the presence of the skyrmion, the term (8) should be taken into account. As pointed out above, for small skyrmion size $\xi_{sc} \gg R$, the skyrmion field can be approximated as a local magnetic impurity with

$V(\boldsymbol{r}) = S_{\rm e}\,\sigma_z\delta^2(\boldsymbol{r})$[1]. Such a local perturbation can be treated exactly by calculating the T-matrix

$$T(\omega) = \frac{-S_{\rm e}\sigma_z}{1 + S_{\rm e}\sigma_z g_0(\omega)} \tag{9}$$

taken into account in T-matrix calculation, which gives the following SP-LDOS at the skyrmion core

$$\rho_s(\omega) = \tag{10}$$
$$-\frac{1}{\pi}\,\mathrm{Im\,Tr}\left\{\frac{1+\tau_z}{2}\,\frac{1+\sigma_s}{2}\,[g_0(\omega) + g_0(\omega)T(\omega)g_0(\omega)]\right\},$$

where energy has infinitesimally small imaginary part in the right side of the equation, i.e. $\omega \to \omega + i\delta$, and $s = x, y, z$ denotes the spin quantization axis. In Eqs. (9) and (10), the $g_0(\omega)$ is the on-site matrix element of the Green's function $g(\omega, \boldsymbol{p}) = [\omega - h(\boldsymbol{p})]^{-1}$

$$g_0(\omega) = -\pi\rho \sum_{\lambda=\pm1} \frac{1+\lambda\sigma_z}{2}\,\frac{\omega - \lambda S + \Delta\tau_x}{\sqrt{\Delta^2 - (\omega - \lambda S)^2}}, \tag{11}$$

where $\rho = m/2\pi$ is the density of states. We plot LDOS (10) in Fig. 2(b). We observe that the skyrmion-YSR (SYSR) states split from the bulk bands. The energy of the states is given by the poles of the T-matrix, i.e. satisfy the equation $1 + S_{\rm e}\sigma_z g_0(\omega) = 0$, which gives

$$E^{\pm}_{\rm SYSR} = \pm\left[S + \Delta\frac{1 - (\pi\rho S_{\rm e})^2}{1 + (\pi\rho S_{\rm e})^2}\right]. \tag{12}$$

The SYSR states maintain the spin polarization of the bands they split off: the positive (negative) SYSR state "up" ("down") spin-polarized. For small skyrmions $R \sim 1/p_F$, the effective magnetic moment of a skyrmion $S_{\rm e}$ is small, and, so, the SYSR states are close to the outter coherence peaks $\pm(\Delta + S)$ as seen in Fig. 2(b). Therefore the SYSR states lie inside continuum of states with the opposite spin. In the absence of coupling between the spin-"up" and "down" sectors of the Hamiltonian, the SYSR states do not mix with the background delocalized states and maintain zero spectral width. In this respect, they do not differ much from the conventional YSR states.

In such a way, we have shown that the skyrmion can be treated as a point impurity and induces a YSR-like state in the spectrum. Let us now expand the model by taking into account that the in-plane spins, which are unavoiably present around the skyrmion, can couple the up and down sectors of the Hamiltonian. As discussed above, the in-plane spins are characterized by

[1] Using Eqs. (2) and (3), the moments can be expressed via the original parameters of the model as $S_{\rm e} = c_1 SR^2$ and $S_{\rm m} = c_2 SR^3$, where S is ferromagnetic coupling and R - the skyrmion radius. The coefficients $c_1 \approx 5.18$ and $c_2 \approx 6.53$ are calculated in the Supplementary Material for a specific model.

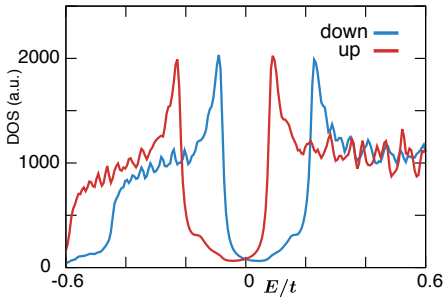

FIG. 3. Spin-resolved density of states obtained by a numerical calculation. Bunch of states are found inside of the superconducting gap in each spin sector. The expected sYSR states get buried in the continuum states with the opposite spin component.

the first moment tensor Eq. (3). In the case of the hedgehog skyrmion, the tensor only contains the diagonal component corresponding to the monopole moment $S_{\rm m}$. Therefore we modify the local perturbation describing the skyrmion as $V(\boldsymbol{r}) = S_{\rm e}\,\sigma_z\delta^2(\boldsymbol{r}) - S_{\rm m}\,\boldsymbol{\sigma}\cdot\boldsymbol{\nabla}\delta^2(\boldsymbol{r})$. We repeat the T-matrix calculation for this perturbation in the Supplementary Material and obtain

$$T(\omega) = \frac{-S_{\rm e}\sigma_z + S_{\rm m}^2 p_F^2 \bar{g}_0(\omega)}{1 + S_{\rm e}\sigma_z g_0(\omega) - S_{\rm m}^2 p_F^2\,\bar{g}_0(\omega)\,g_0(\omega)}, \tag{13}$$

where for brevity $\bar{g}_0(\omega) = \frac{1}{2}\sum_{j=x,y}\sigma_j g_0(\omega)\sigma_j$ is the Green's function obtained from Eq. (11) by substitution $\sigma_z \to -\sigma_z$. We compare Eqs. (9) and (13) and observe that the latter contains renormalized numerator and the denominator due to S_m. We substitue the T-matrix (13) in Eq. (10) and plot LDOS in Fig. 2(c). We observe the LDOS around the SYSR state has significantly widened. In order to explain this, let us consider poles of the T-matrix (13) given by $1 + S_{\rm e}\sigma_z g_0(\omega) - S_{\rm m}^2 p_F^2\,\bar{g}_0(\omega)\,g_0(\omega) = 0$. The real part of this equation still gives the SYSR state given by Eq. (12). However, since $\bar{g}_0(\omega)$, which is the Green's function for a flipped spin, is imaginary at the SYSR energy, the term $S_{\rm m}^2 p_F^2\,\bar{g}_0(\omega)\,g_0(\omega)$ becomes imaginary and determines a finite spectral width of SYSR resonance. The LDOS also manifests an upshoot This explains the apparent widening of the spectrum around the SYSR state. The LDOS even contains an upshoot around the inner coherence peaks $\pm(\Delta - S)$.

Numerical analysis. The above discussed system can be analysed with a tight-binding model. The substrate superconductor is described by a square lattice with energy transfer among the neighboring sites, the chemical potential, and on-site superconducting pairing which are denoted by t, μ, and Δ, respectively.

$$H = \sum_{\langle i,\,j\rangle,\,\sigma} -tc^\dagger_{i\sigma}c_{j\sigma} + \sum_{i,\,\sigma}(2t - \mu)c^\dagger_{i\sigma}c_{i\sigma} \tag{14}$$
$$+ \sum_i(\Delta c^\dagger_{i\uparrow}c^\dagger_{i\downarrow} + \text{h.c.}) + \sum_{i,\,\alpha\beta} JSc^\dagger_{i\alpha}\boldsymbol{S}\cdot\boldsymbol{\sigma}_{\alpha\beta}c_{j\beta} \tag{15}$$

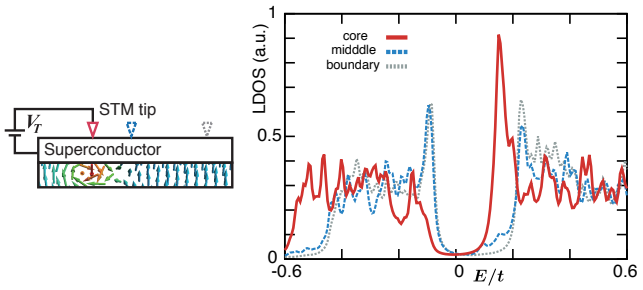

FIG. 4. (Color online) Spin-resolved local density of states with a conceptual cartoon of the experimental setup. The curves show the local density of states with the down spin component at the points corresponding to the position of the STM tips.

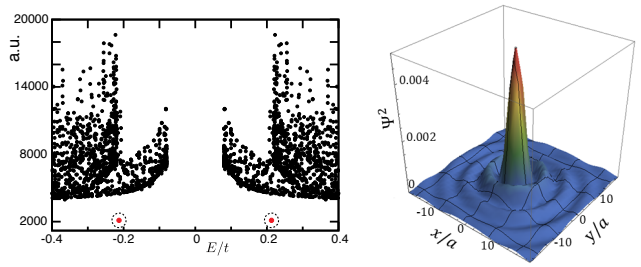

(a) (b)

FIG. 5. (Color online) (a) IPR of each eigen energy eigenstates obtained by the numerical calculation. The dots highlighted by red (encircled by dotted line) correspond to the localized states around the core of the skyrmion, which are identified as sYSR states. (b) Numerical wavefunction corresponding to the sYSR state. The wave function has pronounced oscillations with a period of approximately the superconducting coherence length. Parameters used here are shown in the main text.

Here we employ $f(r) = \pi - 4\arctan\exp(-r/R)$ with $R = 2.5$ as a profile function determining the shape of the skyrmion, which behaves as $f(r = 0) = 0$ and $f(r \to \infty) = \pi$. The moment at the site i is represented by

$$\boldsymbol{S}(\boldsymbol{r}_i) = \begin{pmatrix} y_i \sin(f(r_i))/r_i \\ -x_i \sin(f(r_i))/r_i \\ \cos(f(r_i)) \end{pmatrix}, \tag{16}$$

where x_i and y_i are spatial coordinate measured from the core of the skyrmion and $r_i = \sqrt{|\boldsymbol{r}_i|^2}$. The parameters are chosen as $t = 1.0$, $\mu = 0.5$, $\Delta = 0.15$, and $JS = 0.07$ so that the system has good consistency with the continuum description and the superconducting coherent length is long enough compared with the size of the skrmion. The up Figure 3 shows the spin-resolved density of states in the system. The up-spin(down-spin) components are shifted downward(upward) in energy due to the coupling with the ferromagnetic background. Another feature one can easily see from the figure is that there exist group of states inside the superconducting gap in each spin sector. They are exactly bound states we discussed in the last chapters. The moments surrounding the skyrmion core have finite in-plane components, which produces mixing between two spin sectors. This is the major reason why the peaks are broadened unlike the sharp peaks of simple Shiba states. The inverse participation ratio (IPR) demonstrates this picture, which is defined as

$$\text{IPR} = \frac{1}{\sum_i |\psi(\boldsymbol{r}_i)|^4}, \tag{17}$$

where $\psi(\boldsymbol{r}_i)$ is the amplitude of the wavefunction at the site $\boldsymbol{r}_i$. The IPR helps us to extract the localized states from the mass of continuum states since it scales proportional to $1/L^2$ when the wavefunction ψ is extended throughout the system whereas it has a constant value when ψ is localized at a certain area in the system. Figure 5 showing IPR of each eigenfunction around at the energy close to 0 display two distinct points apart from the others.

Conclusion There are two effects: local scattering and Zeeman field hence the DOS will be split etc. Draw similarities and differences with single imp. In parallel with skyrmion discovery the local imaging using magnetic probes like MFM and SP-STM allowed one to image the matter at atomic resolution while also resolving spin content of electron carriers in the substrate. Here we prove the existence of the new type of localized excitation on the skyrmion core we call Sc-YSR state (alternative is skyrmion bound state (sbs)). Show the main results upfront in the introduction. Both LDOS and SP-LDOS.

[1] N. Y. Yao, L. I. Glazman, E. A. Demler, M. D. Lukin, and J. D. Sau, "Enhanced Antiferromagnetic Exchange between Magnetic Impurities in a Superconducting Host," Phys. Rev. Lett. **113**, 087202 (2014).

[2] G. C. Ménard, S. Guissart, C. Brun, S. Pons, V. S. Stolyarov, F. Debontridder, M. V. Leclerc, E. Janod, L. Cario, D. Roditchev, P. Simon, and T. Cren, "Long range coherent magnetic bound states in superconductors," arXiv:1506.06666.

[3] S. Heinze, K. von Bergmann, M. Menzel, J. Brede, A. Kubetzka, R. Wiesendanger, G. Bihlmayer, and S. Blügel, "Spontaneous atomic-scale magnetic skyrmion lattice in two dimensions," Nat. Phys. **7**, 713 (2011).

[4] N. Romming, C. Hanneken, M. Menzel, J. E. Bickel, B. Wolter, K. von Bergmann, A. Kubetzka, and R. Wiesendanger, "Writing and deleting single magnetic skyrmions," Science **341**, 636 (2013).

[5] K. von Bergmann, A. Kubetzka, O. Pietzsch, and R Wiesendanger, "Interface-induced chiral domain walls,

spin spirals and skyrmions revealed by spin-polarized scanning tunneling microscopy," J. Phys.: Condens. Matter **26**, 394002 (2014).
[6] J. Brede, N. Atodiresei, V. Caciuc, M. Bazarnik, A. Al-Zubi, S. Blügel, and R. Wiesendanger, "Long-range magnetic coupling between nanoscale organic-metal hybrids mediated by a nanoskyrmion lattice," Nat. Nanotechnol. **9**, 1018 (2014).
[7] A. Sonntag, J. Hermenau, S. Krause, and R. Wiesendanger, "Thermal stability of an interface-stabilized skyrmion lattice," Phys. Rev. Lett. **113**, 077202 (2014).
[8] K. von Bergmann, M. Menzel, A. Kubetzka, and R. Wiesendanger, "Influence of the local atom configuration on a hexagonal skyrmion lattice," Nano Lett. **15**, 3280 (2015).
[9] N. Romming, A. Kubetzka, C. Hanneken, K. von Bergmann, and R. Wiesendanger, "Field-dependent size and shape of single magnetic skyrmions," Phys. Rev. Lett. **114**, 177203 (2015).
[10] L. Yu, "Bound state in superconductors with paramagnetic impurities," Acta Phys. Sin. **21**, 75 (1965).
[11] H. Shiba, "Classical Spins in Superconductors," Prog. Theor. Phys. **40**, 435 (1968).
[12] A. I. Rusinov, JETP Lett. **9**, 85 (1969).
[13] A. V. Balatsky, I. Vekhter, and J.-X. Zhu, "Impurity-induced states in conventional and unconventional superconductors," Rev. Mod. Phys. **78**, 373 (2006).
[14] S. Nakosai, Y. Tanaka, and N. Nagaosa, "Two-dimensional p-wave superconducting states with magnetic moments on a conventional s-wave superconductor," Phys. Rev. B **88**, 180503 (2013).

Appendix A: T-matrix analysis

In this section, we give an analytic treatment of the skyrmion-induced bound states using the T-matrix approximation. Starting from the Hamiltonian (5) in the second-quantized form, we write the Bogolyubov-de Gennes (BdG) Hamiltonian as

$$\begin{aligned} &H_{\rm BdG} = H(\boldsymbol{p}) + V(\boldsymbol{r}), \quad \text{where} \\ &H(\boldsymbol{p}) = \xi(\boldsymbol{p})\tau_z + \Delta\tau_x - \boldsymbol{S}(\infty)\cdot\boldsymbol{\sigma}, \quad \boldsymbol{S}(\infty) = -S\,\hat{\boldsymbol{z}}, \\ &V(\boldsymbol{r}) = -\left[\boldsymbol{S}(\boldsymbol{r}) - \boldsymbol{S}(\infty)\right]\cdot\boldsymbol{\sigma} \end{aligned} \tag{A1}$$

The momentum-dependent part $H(\boldsymbol{p})$ describes a superconductor coupled to a spatially uniform ferromagnetic vector $\boldsymbol{S}(\infty)$, whereas the position-dependent piece $V(\boldsymbol{r})$ describes the local perturbation due to the skyrmion. Although the specific model is not significant, we assume the following model for the skyrmion centered at the origin $r = 0$

$$\begin{aligned} &\boldsymbol{S}(\boldsymbol{r}) = S\left[\cos\phi(\boldsymbol{r})\sin\theta(\boldsymbol{r}),\, \sin\phi(\boldsymbol{r})\sin\theta(\boldsymbol{r}),\, \cos\theta(\boldsymbol{r})\right], \\ &\phi(\boldsymbol{r}) = \arctan(x/y), \quad \theta(\boldsymbol{r}) = \pi\left[1 - \exp\left(-\frac{r^2}{R^2}\right)\right], \end{aligned} \tag{A2}$$

where $\phi(\boldsymbol{r})$ and $\theta(\boldsymbol{r})$ denote the polar and azimuthal angle of the vector $\boldsymbol{S}(\boldsymbol{r})$, and R controls the skyrmion size. The superconducting coherence length is usually greater than a typical skyrmion size $R \sim 5\,\text{nm}$ [3–9], i.e. $\xi_{\rm sc} \gg R$. Therefore, the superconductivity does not "resolve" the fine details of the skyrmionic configuration of the field $\boldsymbol{S}(\boldsymbol{r})$, but rather "sees" its long-wavelength characteristics such as the moments described by Eqs. (2) and (3). Motivated by this logic, we substitute the original skyrmionic field $\boldsymbol{S}(\boldsymbol{r})$ by its local version

$$\boldsymbol{S}(\boldsymbol{r}) - \boldsymbol{S}(\infty) = \left[S_{\rm e}\,\hat{\boldsymbol{z}} - S_{\rm m}\,\boldsymbol{\nabla}\right]\delta^2(\boldsymbol{r}). \tag{A3}$$

Here, in order to relate the moments to the original parameters of the model we subtitute Eq. (A2) in Eqs. (2) and (3) and find

$$S_{\rm e} = SR^2\pi\left[-\text{Ci}(\pi) + \gamma + \log(\pi)\right] \approx 5.18\,SR^2, \tag{A4}$$

$$S_{\rm m} = SR^3\int_0^\infty 2\pi t^2 \sin\left(\pi e^{-t^2}\right)\,dt \approx 6.53\,SR^3. \tag{A5}$$

Equation (A3) is convenient for the T-matrix calculation, which we now proceed to. We take into account (A3) and calculate the Fourier transform of Eq. (A1)

$$V(\boldsymbol{p}) = -S_{\rm e}\,\sigma_z + i\,S_{\rm m}\,\boldsymbol{\sigma}\cdot\boldsymbol{p}, \tag{A6}$$

using which we write an intergal equation for the T-matrix

$$\begin{aligned} T\left(\boldsymbol{p}^1, \boldsymbol{p}^2\right) &= V\left(\boldsymbol{p}^1 - \boldsymbol{p}^2\right) \\ &+ \int d^2p'\,V\left(\boldsymbol{p}^1 - \boldsymbol{p}'\right) g(\omega, \boldsymbol{p}')T\left(\boldsymbol{p}', \boldsymbol{p}^2\right). \end{aligned} \tag{A7}$$

Here, the bare Green's function of the superconductor is defined as

$$g(\omega, \boldsymbol{p}) = \frac{1}{\omega - H(\boldsymbol{p})} = \frac{1}{\omega - \xi(\boldsymbol{p})\tau_z - \Delta\tau_x - S\sigma_z}. \tag{A8}$$

Since in the case of the superconductivity we are interested in the scatterings close to the Fermi surface, we use $\boldsymbol{p}^1 = p_F\,\boldsymbol{n}^1$ and $\boldsymbol{p}^2 = p_F\,\boldsymbol{n}^2$, where the in-plane unit vectors $\boldsymbol{n}^1$ and $\boldsymbol{n}^2$ determine the direction of scattering on the Fermi surface. Then, we seek the T-matrix in the following form

$$T\left(\boldsymbol{n}^1, \boldsymbol{n}^2\right) = A + B_i n_i^1 + C_i n_j^2 + D_{ij} n_i^1 n_j^2, \tag{A9}$$

where A, B_i, C_i and D_{ij} are the matrices in the four-components space $\sigma \otimes \tau$. We substitute ansatz (A9) in the integral Eq. (A7) and find the T-matrix

$$T\left(\boldsymbol{n}^1,\boldsymbol{n}^2\right)=\frac{-S_{\rm e}\sigma_z+S_{\rm m}^2p_F^2\bar{g}_0(\omega)+i\,S_{\rm m}\,p_F\,\boldsymbol{\sigma}\cdot(\boldsymbol{n}^2-\boldsymbol{n}^1)+S_{\rm m}^2\,p_F^2\,\bar{g}_0(\omega)\,\left(\boldsymbol{\sigma}\cdot\boldsymbol{n}^2\right)\,\left(\boldsymbol{\sigma}\cdot\boldsymbol{n}^1\right)}{1+S_{\rm e}\sigma_z g_{00}-S_{\rm m}^2p_F^2\,\bar{g}_0(\omega)\,g_0(\omega)},\tag{A10}$$

where the Green's function on-site matrix element in the real space is denoted as

$$\begin{aligned}g_0(\omega)&=\int d^2p\,g(\omega,\boldsymbol{p})\qquad\qquad(A11)\\&=-\pi\rho\sum_{\lambda=\pm1}\frac{1+\lambda\sigma_z}{2}\,\frac{\omega-\lambda S+\Delta\tau_x}{\sqrt{\Delta^2-(\omega-\lambda S)^2}},\\\bar{g}_0(\omega)&=\frac{1}{2}\sum_{j=x,y}\sigma_j\,g_0(\omega)\,\sigma_j.\qquad\qquad(A12)\end{aligned}$$

For brevity, $\bar{g}_0$ denotes the Green's function obtained from g_{00} by replacing $\sigma_z\to-\sigma_z$ according to Eq. (A12). The density of states per spin is denoted as $\rho=m/2\pi$.

1. LDOS

So, in the presence of the skyrmion, the Green's function becomes

$$\begin{aligned}G(\omega,\boldsymbol{p}^1,\boldsymbol{p}^2)=&g(\omega,\boldsymbol{p}^1)\,(2\pi)^2\delta(\boldsymbol{p}^1-\boldsymbol{p}^2)\\&+g(\omega,\boldsymbol{p}^1)T(\boldsymbol{p}^1,\boldsymbol{p}^2)g(\omega,\boldsymbol{p}^2),\end{aligned}\tag{A13}$$

using which the spin-polarized local density of states (LDOS) can be expressed

$$\begin{aligned}\rho_s(\omega,\boldsymbol{r})=-\frac{1}{\pi}\,{\rm Im}\lim_{\omega\to\omega+i\delta}{\rm Tr}\Bigg[&\frac{1+\tau_z}{2}\,\frac{1+\sigma_s}{2}\\&\int\frac{d^2p^1\,d^2p^2}{(2\pi)^4}e^{i(\boldsymbol{p}^1-\boldsymbol{p}^2)\boldsymbol{r}}G(\omega,\boldsymbol{p}^1,\boldsymbol{p}^2)\Bigg]\end{aligned}\tag{A14}$$

where $s=x,y,z$ denotes the spin quantization axis. It can be easily evaluated for instance at the skyrmion core, i.e., at $\boldsymbol{r}=0$,

$$\begin{aligned}\rho_s(\omega,0)=-\frac{1}{\pi}\,{\rm Im}\lim_{\omega\to\omega+i\delta}{\rm Tr}\Bigg\{&\frac{1+\tau_z}{2}\,\frac{1+\sigma_s}{2}\\&\left[g_0(\omega)+g_0(\omega)\frac{-S_{\rm e}\sigma_z+S_{\rm m}^2p_F^2\bar{g}_0(\omega)}{1+S_{\rm e}\sigma_z g_{00}-S_{\rm m}^2p_F^2\,\bar{g}_0(\omega)\,g_0(\omega)}g_0(\omega)\right]\Bigg\}\end{aligned}\tag{A15}$$

2. Spatial wave function

Appendix B: Log range wavefunction of sYSR states

As we discuss in the main text, the sYSR states are different from the ordinary YSR state in that their wavefunctions decay in a power-law on the spatial coordinate. Figure 7 shows the sYSR wavefunction in the log-log scale. One can see the envelope of it linearly decays along the separation from the core of the skyrmion. The calculation was done in the system with 100×100 sites with open boundary condition and the skyrmion is sitting at the center. The deviation from the power-law decay around $r\sim30$ and further will be attributed from the effect of the boundaries.

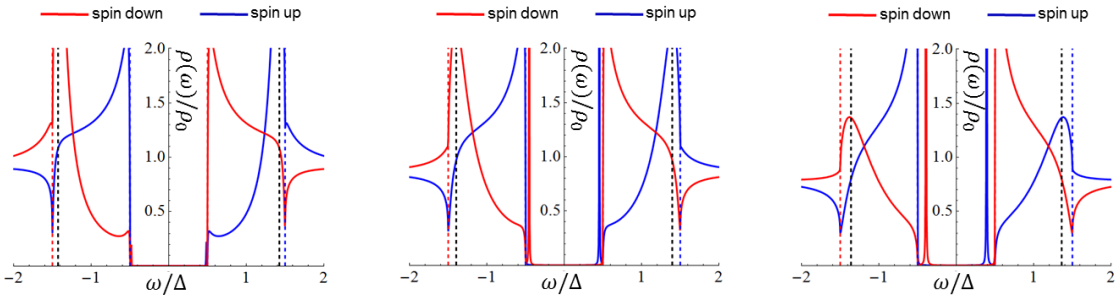

FIG. 6. (Color online) Spin-polarized local density of states (SP-LDOS) at the core of the skyrmion. The consequent panels correspond to increasing skyrmion size (a) $R = 1.1p_F^{-1}$, (b) $R = 1.2p_F^{-1}$, (c) $R = 1.3p_F^{-1}$. Other parameters are the same as in Fig. 2.

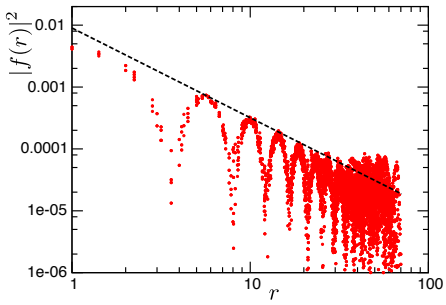

FIG. 7. The spatial dependence of the sYSR wavefunction, which shows the power-law. The break line shows $g(r) = ar^{-b}$ for the guide of eyes ($a = 0.009$ and $b = 1.45$ in this case).